

## Reaction of porphyrin-based surface-anchored metal-organic frameworks to prolonged illumination

Michael Adams<sup>1</sup>, Nicolò Baroni<sup>1</sup>, Michael Oldenburg<sup>1</sup>, Felix Kraffert<sup>2</sup>, Jan Behrends<sup>2</sup>, Rowan W. MacQueen<sup>3</sup>, Ritesh Haldar<sup>6</sup>, Dmitry Busko<sup>1</sup>, Andrey Turshatov<sup>1</sup>, Ganapathi Emandi<sup>5</sup>, Mathias O. Senge<sup>5</sup>, Christof Wöll<sup>6</sup>, Klaus Lips<sup>2,4</sup>, Bryce S. Richards<sup>1,7</sup>, Ian A. Howard<sup>1,7</sup>

1. Institute of Microstructure Technology, Karlsruhe Institute of Technology, Eggenstein-Leopoldshafen, Germany.
2. Fachbereich Physik, Freie Universität Berlin, Berlin Joint EPR Lab, Berlin, Germany.
3. Institute for Nanospectroscopy, Helmholtz-Zentrum Berlin für Materialien und Energie GmbH, Berlin, Germany.
4. Helmholtz-Zentrum Berlin für Materialien und Energie GmbH, Berlin Joint EPR Lab, Berlin, Germany.
5. School of Chemistry, Trinity Biomedical Sciences Institute, Trinity College Dublin, The University of Dublin, Dublin, Ireland
6. Institute of Functional Interfaces, Karlsruhe Institute of Technology, Eggenstein-Leopoldshafen, Germany.
7. Light Technology Institute, Karlsruhe Institute of Technology, Karlsruhe, Germany.

## Time-resolved 2D EPR spectra

The following plots show the full trEPR spectra with both time and spectral information. The graphs shown in the main text contain time slices for the given delay times after the laser excitation extracted from the datasets presented here.

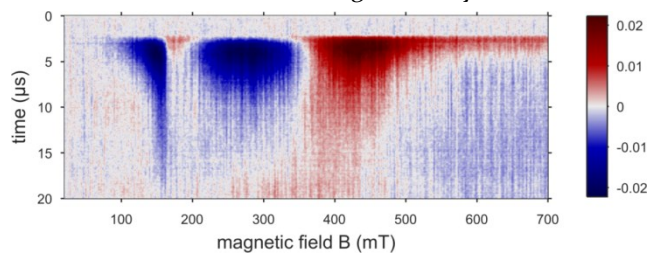


Figure S1: X-band trEPR data of PdTPP (0.5 mM in toluene).

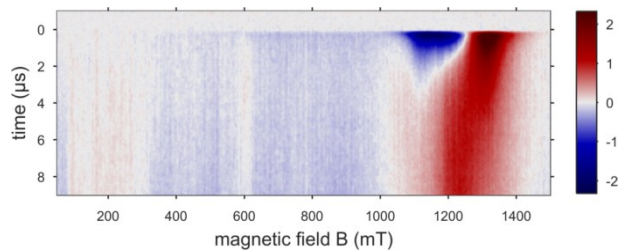


Figure S2: Q-band trEPR data of PdTPP (0.5 mM in toluene).

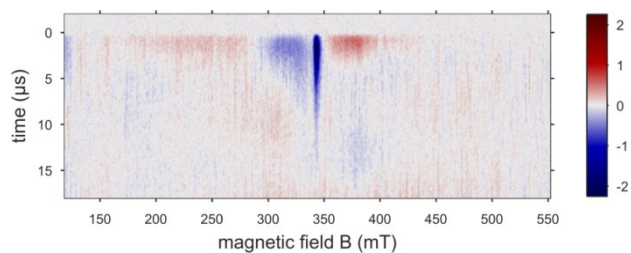


Figure S3: X-band trEPR data of PdP SURMOF thin film.

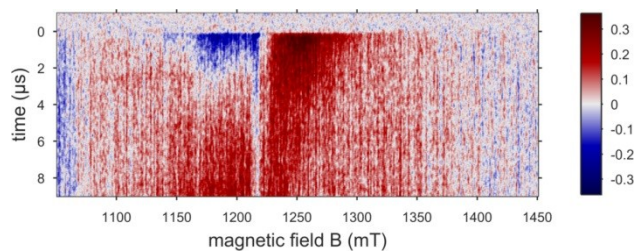


Figure S4: Q-band trEPR data of PdP SURMOF thin film.

## Comparison of late-time model and experimental trEPR spectra

The same spin systems used to fit the early portions of the spectra were applied to later time-slices, allowing only spin polarisation to change, to indicate consistency of the spin system model.

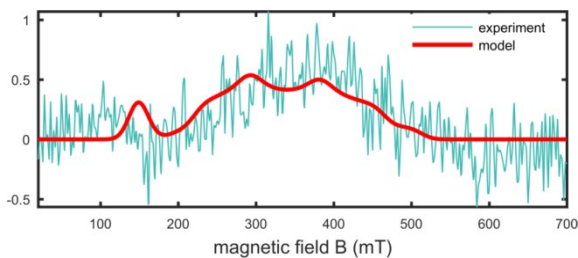


Figure S5: X-band trEPR spectra of PdTPP (0.5 mM in toluene), 18  $\mu$ s after excitation. Triplet spectrum is nearly thermalized to 20K.

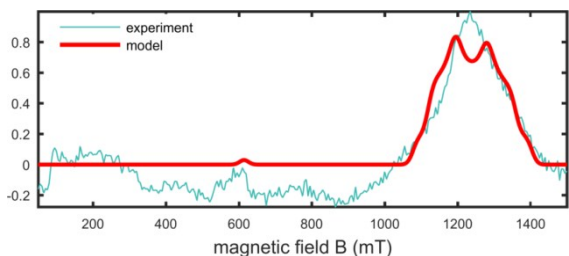


Figure S6: X-band trEPR spectra of PdTPP (0.5 mM in toluene), 9  $\mu$ s after excitation. Thermalisation to 20K is nearly complete. The signal in the lower field region is an experiment artifact that is invariant with time delay.

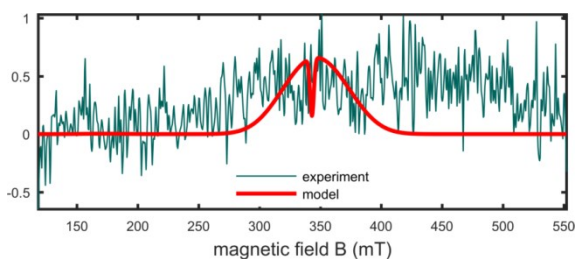


Figure S7: X-band trEPR spectra of PdP SURMOF 18  $\mu$ s after excitation. The signal has effectively degraded to zero and the spectrum is dominated by background noise. The model system is drawn to indicate peak location.

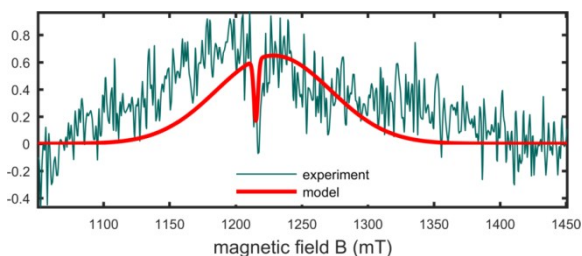


Figure S8: Q-band trEPR spectra of PdP SURMOF 9  $\mu$ s after excitation. The radical signal persists and the triplet has partially thermalized. The model drawn is for the fully-thermalised triplet exciton.

## TAS model single-component spectra

The data from a transient absorption spectroscopy can be represented by a  $N \times M$  matrix  $D$ , where one direction corresponds to the  $M$  discrete wavelength values and the other to the  $N$  time values. Assuming that the data matrix can be described by  $P$  species (in other words: the rank of  $D$  is  $P$ ), it can be decomposed into matrices  $S$  (a  $M \times P$  matrix) and  $C$  (a  $N \times P$  matrix) that contain the profiles of the spectra and the time-evolution of the concentrations, respectively:

$$D = CS^T. \quad (S_1)$$

In our case, we have two species (triplets and radicals) and  $P=2$ . After calculating the relative radical pair concentration using the model described in the main manuscript, we are able to construct  $C$ . We now can solve the linear equation system in eq. S1 for  $S$ , using  $C$ , and the experimental data as  $D$ . We concatenate  $D$  and  $C$  for all excitation fluences, as their spectra should be identical. As we are dealing with experimental data, eq. S1 does not have an exact solution in our case but we can use the MATLAB function *mrdivide* to obtain an approximate least-square solution.

The resulting spectra for the two components (triplets and radical pairs) are shown in Fig. S9. The main feature of the radical species is indeed the GSB in the 605-620 nm wavelength region. However, the TAS signal in this region is overlaid with a nonzero negative signal (PIA) from the triplet exciton population. This is consistent with our earlier observation that the TAS signal in this region is determined by triplet PIA at early times (<20 ns) and becomes dominated by radical GSB afterwards. Furthermore, the triplet population can ideally be tracked by its PIA in the wavelength region below 500 nm, as the radical signal is small in this wavelength region.

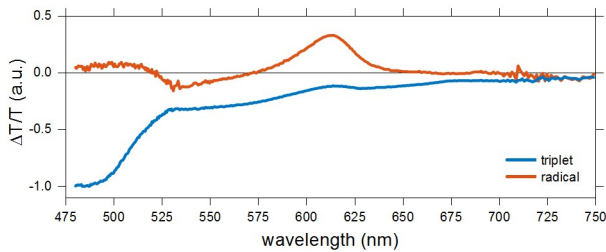


Figure S9: Single-component spectra for the two components that make up the experimental data matrix  $D$ . The scale of both spectra is arbitrary.

## Supplementary TAS figures

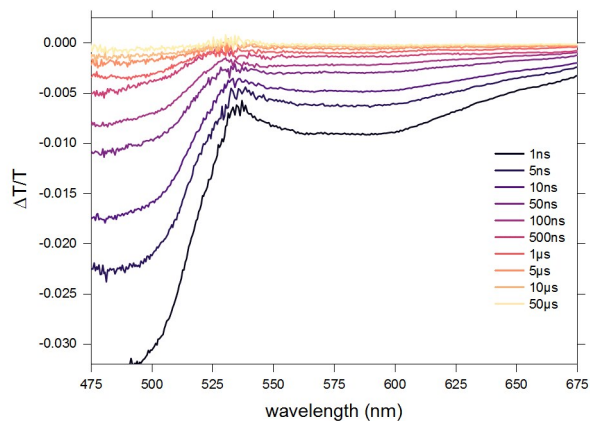


Figure S10: TAS spectra at different pump-probe delay times for a PdP SURMOF before photodegradation and excited with the 532 nm pulsed pump laser at  $120 \mu\text{J}/\text{cm}^2$  (500 Hz repetition rate). This is an alternative representation of the data presented in Figure 1A in the main document.

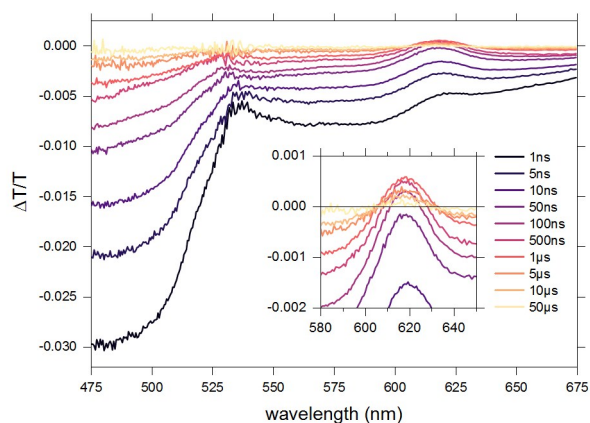


Figure S11: TAS spectra at different pump-probe delay times for a PdP SURMOF after 15.4 hours of photodegradation with the 532 nm pulsed pump laser at  $120 \mu\text{J}/\text{cm}^2$  (500 Hz repetition rate). This is an alternative representation of the data presented in Figure 1B in the main document. The inset zooms in on the new GSB introduced by continuous illumination.

## SURMOF structure

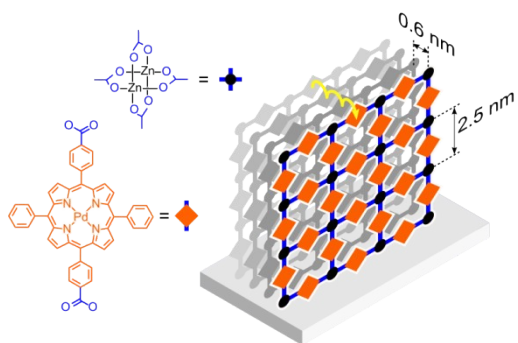


Figure S12: Chemical structure of the Pd-porphyrin linker molecule (orange) and the zinc paddlewheel metal center (black) as well as a schematic drawing of the PdP SURMOF showing the arrangement of the linker and metal center into sheets that stand on the substrate. The yellow line shows the preferential direction of triplet migration between SURMOF sheets by Dexter transfer (hopping).

### Structural characterization of pristine and illuminated PdP SURMOF by X-Ray Diffraction (XRD)

We measured the XRD spectrum of a PdP SURMOF thin film sample in pristine conditions and after 15 hours of illumination. The sample was kept under dynamic vacuum ( $<10^{-4}$  Pa) at room temperature and illuminated with a 405 nm CW laser at a power density of  $0.1 \text{ W/cm}^2$  for several hours. In total, we calculate that around  $2 \times 10^{27} \text{ photons cm}^{-3}$  were absorbed by the sample.

The most prominent features in the pristine SURMOF's out-of-plane XRD spectra (see Figure S13) are the (002) diffraction peak at  $2\theta=7.1^\circ$  and the (001) diffraction peak at  $2\theta=3.4^\circ$ . The peak positions are consistent with literature<sup>1</sup> and correspond to the intrasheet distance between two porphyrin chromophores of 2.5 nm. The out-of-plane XRD data of the SURMOF measured before and after light irradiation does not show any change in the lattice dimension, as can be seen from the unchanged position of the (002) peak. However, the (001) peak intensity vanishes in the irradiated SURMOF, suggesting a change in the lattice form factor. Retention of crystallinity in the irradiated SURMOF suggests that the photoproduct is part of the crystalline structure.

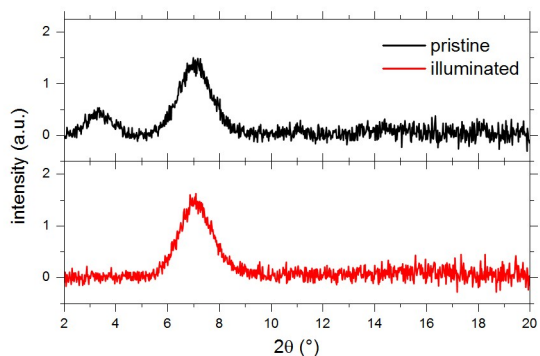


Figure S13: Out-of-plane XRD diffractogram showing the first two orders of the diffraction peak in the (001) and (002) crystalline direction of a pristine PdP SURMOF thin film (top panel, black line) and in a photodegraded PdP SURMOF thin film (bottom panel, red line).

## Changes in absorbance spectrum during illumination

We measured the absorbance spectrum on a PdP SURMOF thin film sample before and after illumination. The sample was kept under dynamic vacuum ( $<10^{-4}$  Pa) at room temperature and excited with a 405 nm CW laser at a power density of  $0.1 \text{ W/cm}^2$  for several hours. After 17 hours, the degradation was interrupted for an absorbance measurement and then continued for another 16 hours. In total, we calculate that around  $9.4 \times 10^{26} \text{ photons cm}^{-3}$  were absorbed by the sample.

Absorption spectra were measured with a UV/vis/NIR spectrophotometer (Perkin-Elmer Lambda 950) in absorbance mode inside an integrating sphere. The obtained spectra are shown in Figure S14. The reduction in Soret- and Q-band absorption is consistent with a reduction in porphyrin concentration caused by a light-induced reaction of Pd-porphyrin to a photoproduct. In contrast to this reduction, absorption slightly increases around 610 nm, which we attribute to the newly formed photoproduct. This is consistent with the observation of a GSB observed in TAS and confirms that the GSB indeed tracks an excited state of the photoproduct. We note again that the position of the 610 nm absorption is consistent with the absorption of Pd-chlorin, which we suggest as a likely candidate for being the photoproduct.

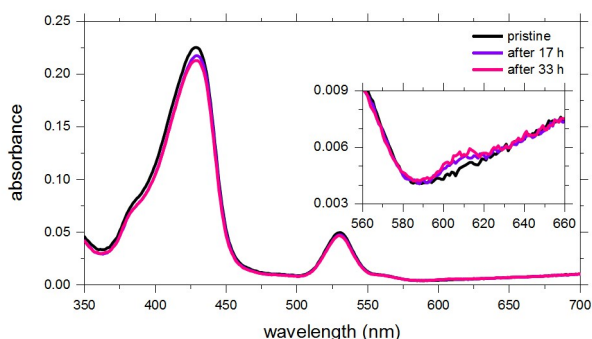


Figure S14: Absorbance spectra of a PdP SURMOF thin film before and after several hours of continuous illumination with a 405 nm CW source at  $0.1 \text{ W/cm}^2$ . The sample was kept under dynamic vacuum at room temperature.

## Characterization of the photoproduct *via* MALDI-ToF

We performed mass spectroscopy by using the MALDI-ToF (matrix-assisted laser desorption/ionization time-of-flight) technique on a PdP SURMOF in pristine condition and after 33 hours of illumination under a 405 nm CW laser at  $0.1 \text{ W/cm}^2$  ( $10^{27}$  absorbed photons per  $\text{cm}^3$ ). Illumination was performed at room temperature under dynamic vacuum ( $<10^{-4}$  Pa).

The mass spectra before and after degradation are shown in Figure S15A and S15B, respectively. We can compare these data to theoretical spectra (Figure S15C-E).<sup>3</sup> The isotopic  $m/z$  distribution for Pd-porphyrin ( $m/z = 807.075$  Da) obtained for a pristine PdP SURMOF resembles the calculated ( $m/z = 807.155$  Da) pattern. The irradiated SURMOF however shows a slight change in the isotopic  $m/z$  distribution, the intensity of  $m/z = 809.967$  Da increases substantially. As the isotopic  $m/z$  distributions of Pd-porphyrin and Pd-chlorin overlap significantly and the photoconversion is only partial, identification of Pd-chlorin  $m/z$  is not straightforward. However, the change in the  $m/z$  intensity distribution is consistent with formation of Pd-chlorin, which is also supported by the spectroscopic measurements.

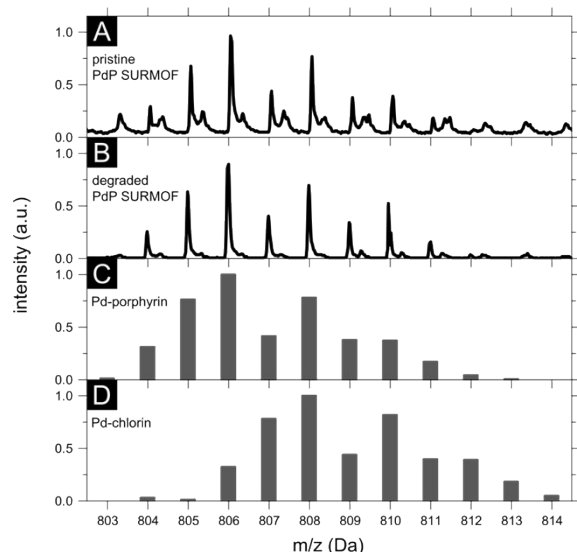


Figure S15: A: Measured MALDI-ToF mass spectrum of a pristine PdP SURMOF thin film sample. B: Measured MALDI-ToF mass spectrum of a PdP SURMOF thin film after 33 hours of illumination. C: Theoretical mass spectrum of Pd-porphyrin (obtained from <http://www.chemcalc.org><sup>3</sup>) for reference. D: Theoretical mass spectrum of Pd-chlorin (obtained from <http://www.chemcalc.org><sup>3</sup>) for reference.

## Synthesis of the PdP linker

See also Fig. S14 for a graphical representation.

### {5,15-Bis(4'-methoxycarbonyl)phenyl-10,20-diphenylporphyrinato}palladium(II) 2

The free base 5,15-bis(4'-methoxycarbonyl)phenyl-10,20-diphenylporphyrin **1** (500 mg, 0.684 mmol) was dissolved in chloroform (50 mL) and mixed with a solution of two equivalents of palladium acetate (306 mg, 1.368 mmol) in methanol (30 mL). The reaction mixture was stirred under an air atmosphere under TLC monitoring (silica gel, n-hexane/CH<sub>2</sub>Cl<sub>2</sub>, v/v, 1:1). A color change from dark red to light pink was observed. The solvent was evaporated under reduced pressure and the red residue dissolved in a small amount of dichloromethane and filtered through a plug of silica gel eluting with n-hexane/CH<sub>2</sub>Cl<sub>2</sub> (2:1, v/v). Alternatively, the same condition was used for column chromatography to give a red solid. Yield: 503 mg (0.603 mmol, 88%). – M.p. >300 °C. – R<sub>f</sub> (CH<sub>2</sub>Cl<sub>2</sub> : hexane, 1:1 v/v) = 0.60 – <sup>1</sup>H NMR (400 MHz, CDCl<sub>3</sub>): δ = 8.83 (d, J = 5.0 Hz, 4H, β-H), 8.75 (d, J = 5.0 Hz, 4H, β-H), 8.43 (d, J = 8.2 Hz, 4H, aryl-H), 8.26 (d, J = 8.2 Hz, 4H, aryl-H), 8.18 (d, J = 8.0 Hz, 4H, aryl-H), 7.80-7.70 (m, 6H, aryl-H), 4.11 ppm (s, 6H, -OCH<sub>3</sub>). – <sup>13</sup>C NMR (150 MHz, CDCl<sub>3</sub>): δ = 167.25, 146.50, 141.73, 141.50, 141.03, 134.10, 134.05, 131.44, 130.67, 129.69, 127.94, 127.89, 126.77, 122.15, 120.58, 52.41 ppm. – UV/Vis (CHCl<sub>3</sub>): λ<sub>max</sub> (log ε) = 416 (5.21), 523 nm (4.02). – HRMS (MALDI): m/z calcd. for [C<sub>48</sub>H<sub>32</sub>N<sub>4</sub>O<sub>4</sub>Pd] 834.1458; found 834.1497.

### {5,15-Bis(4'- carboxyphenyl)-10,20-diphenylporphyrinato}palladium(II) PdP

(5,15-Bis(4'-methoxycarbonyl)phenyl-10,20-diphenylporphyrinato)palladium(II) **2** (300 mg, 0.359 mmol) was dissolved in THF (30 mL) and to this solution KOH (80 mg, 1.436 mmol in 30 mL MeOH) was added. The reaction mixture was heated to 70 °C and was stirred at this temperature for 18 h. Upon complete consumption of the starting material, the reaction mixture was allowed to cool to rt before acidification to pH 4 using 1M HCl. The product was precipitated out and product was washed with distilled water for several times and dried in vacuo to give pink solid. Yield: 265 mg (0.328 mmol, 91%). – M.p. >300 °C. – R<sub>f</sub> (CH<sub>2</sub>Cl<sub>2</sub> : MeOH, 2:1, v/v) = 0.54. – <sup>1</sup>H NMR (400 MHz, DMSO): δ = 13.38 (s, 1H, OH), 8.80 (s, 8H, β-H), 8.34 (d, J = 8.2 Hz, 4H, aryl-H), 8.27 (d, J = 8.1 Hz, 4H, aryl-H), 8.17-8.13 (m, 4H, aryl-H), 7.80-7.76 ppm (m, 6H, aryl-H). – UV/Vis (CH<sub>2</sub>Cl<sub>2</sub>): λ<sub>max</sub> (log ε) = 417 (5.35), 524 nm (4.20). – HRMS (MALDI): m/z calcd. for [C<sub>46</sub>H<sub>28</sub>N<sub>4</sub>O<sub>4</sub>Pd] 806.1145; found 806.1130.

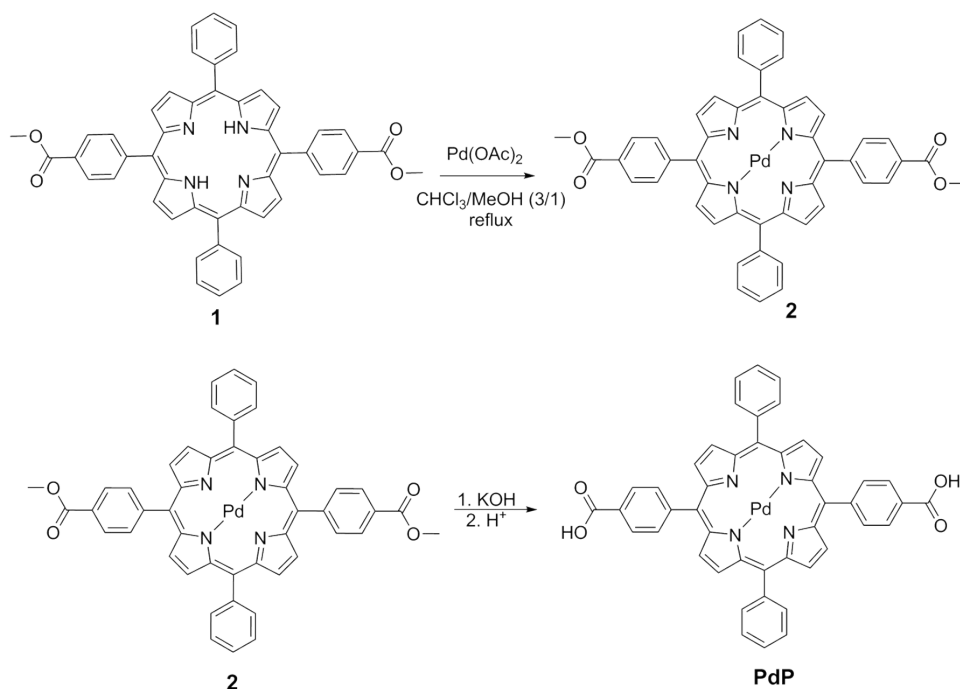


Figure S16: Schematic representation of the linker synthesis steps

## References

- (1) Oldenburg, M.; Turshatov, A.; Busko, D.; Wollgarten, S.; Adams, M.; Baroni, N.; Welle, A.; Redel, E.; Wöll, C.; Richards, B. S.; et al. Photon Upconversion at Crystalline Organic–Organic Heterojunctions. *Adv. Mater.* **2016**, *28* (38), 8477–8482.
- (2) Klug, H. P.; Alexander, L. E. *X-Ray Diffraction Procedures: For Polycrystalline and Amorphous Materials, 2nd Edition*, 2 edition.; Wiley-Interscience: New York, 1974.
- (3) Patiny, L.; Borel, A. ChemCalc: A Building Block for Tomorrow’s Chemical Infrastructure. *J. Chem. Inf. Model.* **2013**, *53* (5), 1223–1228.